Monthly Notices
of the
ROYAL ASTRONOMICAL SOCIETY

MNRAS **469,** 2401–2411 (2017)
Advance Access publication 2017 April 28

doi:10.1093/mnras/stx1020

Statistics of the fractional polarization of compact radio sources in *Planck* maps

Laura Bonavera,[1]★ Joaquin González-Nuevo,[1] Francisco Argüeso[2] and Luigi Toffolatti[1,3]

[1]*Departamento de Física, Universidad de Oviedo, C. Federico García Lorca 18, E-33007 Oviedo, Spain*
[2]*Departamento de Matemáticas, Universidad de Oviedo, Federico García Lorca 18, E-33007 Oviedo, Spain*
[3]*INAF/IASF Bologna, Via Gobetti 101, I-40129 Bologna, Italy*

Accepted 2017 March 28. Received 2017 March 28; in original form 2016 August 6

ABSTRACT

In this work, we apply the stacking technique to estimate the average fractional polarization from 30 to 353 GHz of a primary sample of 1560 compact sources – essentially all radio sources – detected in the 30 GHz *Planck* all-sky map and listed in the second version of the *Planck* Catalogue of Compact Sources (PCCS2). We divide our primary sample in two subsamples according to whether the sources lay (679 sources) or not (881 sources) inside the sky region defined by the *Planck* Galactic mask ($f_{\rm sky} \sim 60$ per cent) and the area around the Magellanic Clouds. We find that the average fractional polarization of compact sources is approximately constant (with frequency) in both samples (with a weighted mean over all the channels of 3.08 per cent outside and 3.54 per cent inside the *Planck* mask). In the sky region outside the adopted mask, we also estimate the μ and σ parameters for the lognormal distribution of the fractional polarization, finding a weighted mean value over all the *Planck* frequency range of 1.0 for σ and 0.7 for μ (that would imply a weighted mean value for the median fractional polarization of 1.9 per cent).

Key words: polarization – radio continuum: galaxies.

1 INTRODUCTION

The polarization properties of extragalactic radio sources (ERS) at frequencies above 10–20 GHz are still poorly constrained by observations. The NRAO Very Large Array (VLA) Sky Survey (NVSS at 1.4 GHz; Condon et al. 1998) still constitutes the largest sample of ERS surveyed both in total flux density, S, and in total linear polarization, P. More recently, the Australia Telescope Compact Array (ATCA), the VLA and other facilities have been extensively used to observe and characterize the polarization properties of ERS sources up to ∼40 GHz. However, extrapolations from these low frequencies up to ∼100 GHz are affected by large uncertainties since a complex combination of effects must be considered. This includes intra-beam effects and bandwidth depolarization, in addition to possible intrinsic frequency-dependent changes (see Tucci et al. 2004; Tucci & Toffolatti 2012, for comprehensive discussions on this subject).

Moreover, extending the knowledge of the polarization properties of ERS is interesting on its own, since it provides information about the physics of the underlying emission process. Thus, to fill this gap of knowledge, in the past decade many intermediate to large samples of ERS have been observed in polarization at frequencies above ≃10 GHz (Sadler et al. 2006; Massardi et al. 2008, 2011, 2013; López-Caniego et al. 2009; Jackson et al. 2010; Murphy et al. 2010; Sajina et al. 2011). All these surveys have provided values of the median fractional polarization of ERS in the range ∼2 per cent to ∼3 per cent of the total flux density of the source. Other recent studies of the polarized emission in ERS have tried to analyse the dependence of the fractional polarization with luminosity, redshift and the source environment. The current, still preliminary, results show no correlation between the fractional polarization and redshift, whereas a weak correlation is found between decreasing luminosity and increasing degree of polarization (see e.g. Banfield et al. 2011).

As reminded above, the total polarization, P, commonly observed in ERS at cm or mm wavelengths is typically a few per cent with only very few ERS showing a total fractional polarization, $\Pi = P/S$, as high as ∼10 per cent of the total flux density (Sajina et al. 2011; Tucci & Toffolatti 2012). However, even this low Π of ERS may constitute a problem for the detection of the primordial polarization in the cosmic microwave background (CMB) maps, since ERS are the dominant polarized foreground at small angular scales and the CMB polarized signal constitutes only a few per cent (e.g. Planck Collaboration XI 2016; Planck Collaboration XIII 2016) of the CMB temperature anisotropy. This very low intrinsic CMB polarized signal means that current experiments are marginally able

★ E-mail: laurabonavera@gmail.com

to detect tensor metric perturbations by the direct detection of the primordial CMB B-mode, but only in the case of very high values of the tensor-to-scalar ratio of primordial perturbations, $r \sim 0.05$–0.1. For this reason, with the most recent available data, only upper limits on the value of r have been obtained (BICEP2/Keck and Planck Collaborations 2015; BICEP2 Collaboration 2016).

Therefore, future CMB all-sky surveys in polarization (e.g. the proposed European Space Agency, ESA, Cosmic ORigin Explorer, CORE, mission, see André, Baccigalupi & Banday 2014, a mission specifically designed to detect the CMB polarization by virtue of a much higher sensitivity than before) – with the capability to reach tensor-to-scalar ratios as low as $r \sim 0.01$ – will surely need a more careful determination of the polarized signal from the (dominant) Galactic diffuse emission but also of the signal coming from ERS (see De Zotti et al. 2015, 2016, for comprehensive reviews on this latter subject). To achieve this goal, a much better characterization of the contaminating signal due to polarized ERS in the CMB anisotropy maps is needed. And this characterization will be only possible by a proper statistical knowledge of the polarization properties of the populations of faint compact sources at mm wavelengths.

This is not an easy task since the current available all-sky catalogues of ERS at mm/sub-mm wavelengths are still limited to the shallow surveys provided by the *Wilkinson Microwave Anisotropy Probe* (*WMAP*) (Bennett et al. 2003) and ESA *Planck* (Planck Collaboration I 2016) missions. The second, updated, version of the *Planck* Catalogue of Compact Sources (PCCS2) (Planck Collaboration XXVI 2016) currently constitutes the deepest complete catalogue of compact radio sources at high frequency (>30 GHz) but, due to the low resolution of the *Planck* beams, it is still limited to very bright sources ($S > 100$ mJy, at the 90 per cent completeness level), even in the cleanest *Planck* channels. Correspondingly, the number of detected compact sources in polarization is very low (only few tens are detected) and their polarization properties are poorly characterized. Moreover, it is obvious that only compact – either Galactic or extragalactic – sources with a high Π can be detected and, thus, the statistical characterization of the underlying population will be biased towards these highly polarized objects. The use of samples of detected compact sources also hampers the possibility of studying the possible variation of Π with the total flux density (Massardi et al. 2013). In particular, the source populations mainly contributing to the source counts down to very faint fluxes could present different Π values as compared to the ones dominating the bright number counts (e.g. Tucci et al. 2004).

To reduce, albeit partially, this lack of data on faint, undetected, compact sources and for better estimating the average fractional polarization, $\langle\Pi\rangle$, of the underlying source population, it is useful to exploit the full information content of the CMB sky maps in polarization by applying stacking techniques, i.e. co-adding the signal from many weak or undetected objects to obtain a statistical detection. Stacking has been already successfully applied to the *Planck* data to search for the ISW signal directly at the positions of positive and/or negative peaks in the gravitational potential, since the expected (and observed) signal is very weak (Planck Collaboration XIX 2014). Moreover, stacking has also been successfully applied to investigate the faint polarized signal of radio sources, detected in total flux density, S, at 1.4 GHz by NVSS. By stacking the polarized signal for NVSS sources down to the detection limit in total flux density the authors (Stil et al. 2014) were able to find a gradual increase – with decreasing flux density – in the median fractional polarization fully consistent with a trend noticed before for bright NVSS sources (Mesa et al. 2002; Tucci et al. 2004).

The outline of the paper is as follows: in Section 2, we discuss the methods adopted for selecting the sky patches, for defining the subsamples, we are going to analyse and for determining their mean fractional polarization; in Section 3, we present our results on the fractional polarisations of compact sources, inside and outside the *Planck* mask, and estimated by stacking; finally, in Section 4, we summarize our main conclusions.

2 METHODS

2.1 Data

Our purpose is to study the main behaviour of compact radio sources in polarization at high frequencies. For this reason, we use the PCCS2 (Planck Collaboration XXVI 2016) catalogue at 30 GHz[1] as our main sample. It consists of 1560 sources above a flux density of 427 mJy at the 90 per cent completeness level (and with a minimum flux of 376 mJy).

We follow these sources in the *Planck* maps at 30, 44, 70, 100, 143, 217 and 353 GHz[1] (Planck Collaboration I 2016), that corresponds to the channels with both total intensity and polarization measurements. Since we are interested in estimating $\langle\Pi\rangle$ and $\langle\Pi^2\rangle$, we generate the P map as the square root of the quadratic sum of the Stokes Q and U parameters maps ($P = \sqrt{Q^2 + U^2}$).

Due to the different behaviour of sources inside and outside the Galactic plane in this wide range of frequencies, we decide to split our sample into two subsamples according to the regions delimited by the *Planck* Galactic mask GAL060 that leaves 60 per cent of the sky unmasked[1]. We also include in the Galactic region a circular sky region of 5° radius around the position of the Large Magellanic Cloud and of 3° radius around the Small Magellanic Cloud.

2.2 Stacking

Stacking is a statistical method that consists in adding up many regions of the sky around previously selected positions (see Dole et al. 2006; Marsden et al. 2009; Béthermin et al. 2012, and references therein). In this way we can reduce the noise/background, since it is expected to fluctuate around the mean with positive and negative values, and enhance the signal we want to study. Stacking is useful when the individual sources in the selected sample are too faint to be detected at the frequency of interest. Therefore, we can measure their mean flux density despite the fact that they are not detectable directly by the given instrument.

In our case we want to perform statistical estimates of polarization with *Planck*. It should be noticed that our target sources are all detected in total intensity at 30 GHz, but they are not necessarily detected in the higher frequency channels: their spectral behaviour is, in fact, typically flat with down-turning spectra above 70 GHz (Planck Collaboration XIII 2011; Planck Collaboration XXVIII 2014). In polarization the situation gets worse since only few tens of sources are detected even at 30 GHz (Planck Collaboration XXVI 2016). For this reason, our scientific case is an excellent application of the stacking methodology.

In particular, with stacking in total intensity and polarization we compute the $\langle\Pi\rangle$ of our source population at frequencies up to

[1] Based on observations obtained with *Planck* (http://www.esa.int/Planck), an ESA science mission with instruments and contributions directly funded by ESA Member States, NASA, and Canada. Available at http://pla.esac.esa.int/pla/#home (*Planck* Legacy Archive).

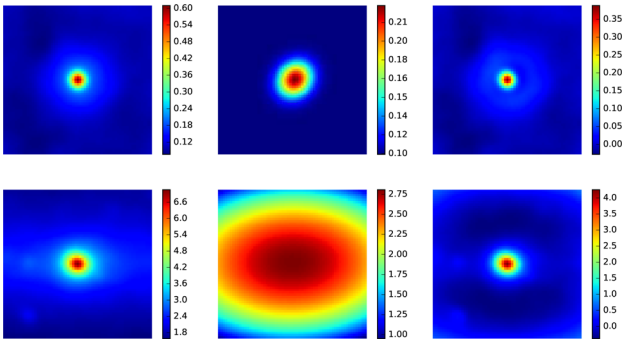

Figure 1. From left to right: mean maps of the original S data, the model fit to the background (see text) and the 'residual' for the 143 GHz channel, outside (top) and inside (bottom) the adopted *Planck* mask. The colour scale is Jy pix^{-1}, the pixel size is 1.72 arcmin and the angular size of the image is 3.14 deg^2. The values in this figure are not yet corrected for the noise bias.

353 GHz (all the *Planck* channels with polarization measurements). To perform stacking, we select a small patch of 63 × 63 pixels (corresponding to ∼40 times the solid angle of the beam at 30 GHz) around each source position. The pixel size is 3.44 arcmin for LFI and 1.72 arcmin for HFI channels. We then add up all the patches to obtain the total flux density. To reduce the instrumental noise (a second order effect) we convolve the resulting patch with a Gaussian filter whose $\sigma_{\rm filter}$ is given by $\sigma_{\rm beam}/2$.

Unlike the case for Stil et al. (2014), where they use high-resolution radio data at 1.4 GHz, in the microwave band and at the much lower *Planck* angular resolution, we need to take into account some additional signals that are plausible contaminants to our stacked measurements: the CMB itself and the diffuse emission of our own Galaxy. Although their contribution is very small in polarization, it is not negligible when stacking over hundreds of targets. In the final stacked image, these small contributions give rise to a strong background signal that has to be removed. Therefore, we estimate and subtract it from the final stacked patch, where the contamination signal can be more easily calculated both in total intensity and in polarization. In polarization, we subtract the mean of the background computed in the external region of the final patch ($3\sigma_{\rm beam}$ away from the patch centre) from the total polarization flux.

In the subsample outside the Galactic mask region, the sources lying on a CMB maximum are more likely to be detected, due to the bias in the source detection in total intensity. In the HFI channels (where the S/N is higher), this fact results in an extended feature around the centre of the final patch. In this latter case, we estimate the background by fitting it with a constant plus Gaussian 2D curve and then subtract it from the data. This effect is clearly not present either in polarization or in our injected sources test (see Section 2.4).

For the subsample inside the Galactic region, due to the Galactic emission gradient, we need to perform a parabolic 2D fit to more carefully estimate the background. We also compute the flux densities in total intensity with the same background subtraction procedure used for polarization and compare both sets of results in Section 3. From these residual maps, we then compute the total flux densities in total intensity and polarization.

An example of background estimation is illustrated in Fig. 1. It refers to the 143 GHz case. On the left, the total intensity map resulting from the stacking in the region outside (top) and inside (bottom) the Galactic mask is shown. The central panel is the model obtained by fitting the background in total intensity. In the top figure, the fit is performed using a flat component and a 2D Gaussian curve to take into account the noisy background and the contribution from the positive CMB fluctuations. In the bottom panel, we use a 2D, two degree polynomial function to model the background in the Galactic region. The right-hand panels show the residual maps that we use to estimate the flux density. It is worth mentioning that in the test with injected sources (described in Section 2.4) there was no need to perform such background fitting, because the boosting effect was not present, strengthening the idea that it is due to a detection bias. It should also be stressed that the values in this figure are not corrected for the noise bias (see Section 2.3).

Finally, we compute $\langle\Pi\rangle = \langle P_0\rangle/\langle S\rangle$, where P_0 is the source total polarization amplitude and $\langle P_0\rangle$ its average over our sample. Its error is given by $\sqrt{(\langle P_0\rangle/\langle S\rangle)^2 \cdot (\sigma^2_{P_0}/\langle P_0\rangle^2 + \sigma^2_S/\langle S\rangle^2)}$, where σ_{P_0} and σ_S are the standard deviations for total intensity and polarization computed in the external region of the stacked patches.

We also compute the quantity $\sqrt{\langle\Pi^2\rangle} = \sqrt{\langle P_0^2\rangle/\langle S^2\rangle}$ by applying the same methodology with the only difference that due to the higher S/N we do not need to perform any background fit to compute $\sqrt{\langle\Pi^2\rangle}$. Its error is given by $\sqrt{\frac{1}{4\langle P_0^2\rangle\langle S^2\rangle}(\sigma^2_{P_0^2} + \langle P_0^2\rangle^2/\langle S^2\rangle^2\sigma^2_{S^2})}$.

Please note that most of our sources are not directly detectable and therefore we cannot estimate directly $\langle\Pi\rangle = \langle P_0/S\rangle$ and $\langle\Pi^2\rangle = \langle P_0^2/S^2\rangle$. For this reason, in our stacking procedure, we decided to calculate $\langle\Pi\rangle = \langle P_0\rangle/\langle S\rangle$ and $\langle\Pi^2\rangle = \langle P_0^2\rangle/\langle S^2\rangle$ that are good approximations for $\langle\Pi\rangle = \langle P_0/S\rangle$ and $\langle\Pi^2\rangle = \langle P_0^2/S^2\rangle$, taking into account that Π and S can be considered independent variables (see e.g. Massardi et al. 2008, 2013 and Galluzzi et al. 2017 as discussed in Section 3.1). Besides, the residual errors introduced by these assumptions are much lower than the noise bias discussed in Section 2.3. Moreover, the bias subtraction methodology described in Section 2.4 also corrects any residual deviation from the theoretical value.

2.3 Noise bias

As stated in Section 2.1, P is a quadratic sum of Q and U. This construction introduces a bias due to the Q and U noise cross-terms. This bias is usually referred as noise bias and it is not negligible for low S/N observations. For this reason, it has to be taken into account in order to correct the measurements. Different methods have been developed for this correction (see e.g. Simmons & Stewart 1985; Vidal, Leahy & Dickinson 2016), but none of them can be directly applied to our case. In fact, in our approach it is important to keep in mind that – by stacking – we are neither observing nor detecting individual sources. This is due to the fact that the polarization signal-to-noise ratio is not high enough to guarantee their direct detection. Moreover the noise bias strongly depends on the S/N that is unknown in our case for each individual compact source. Therefore, in order to get a theoretical estimation of the importance of the noise bias in our procedure, we proceed by considering the n sky patches constructed around the sources detected in the intensity maps and by adding them up in polarization to increase the signal-to noise ratio (stacking method).

As previously discussed, these sources have not been individually detected in the polarization maps. However, we assume that each of these sources is polarized with total polarization amplitude $P_0 = \sqrt{Q_0^2 + U_0^2}$, being Q_0 and U_0 the polarization amplitudes in Q and U, respectively. Far from the centre of the patch – a $3\sigma_{\rm beam}$ distance is enough – we assume that the distribution of the values of Q and U is Gaussian with zero mean and r.m.s deviation $\sigma = \sigma_Q = \sigma_U$, with σ coming from the combination of instrumental noise, CMB and the different foregrounds.

Therefore, in one observed sky patch with no compact sources the polarization $P = \sqrt{Q^2 + U^2}$ follows a Rayleigh distribution (Papoulis 1984) in the pixels outside the source:

$$f(P) = P/\sigma^2 \exp(-P^2/2\sigma^2) \quad (1)$$

On the contrary, if in the central pixel there is a polarized source with total polarization amplitude P_0, we are left with a Rice distribution in P (Rice 1954)

$$f(P) = P/\sigma^2 \exp\left(-(P^2 + P_0^2)/2\sigma^2\right) I_0(P_0 P/\sigma^2) \quad (2)$$

with I_0 the modified Bessel function of order zero. The expectation of P is for the Rayleigh distribution (absence of sources)

$$\mathrm{E}(P) = \sigma \sqrt{\pi/2} \quad (3)$$

and for the Rice distribution (presence of a source)

$$\mathrm{E}(P) = \sigma \sqrt{\pi/2} \exp\left(-P_0^2/4\sigma^2\right) \left[\left(1 + P_0^2/2\sigma^2\right) I_0\left(P_0^2/4\sigma^2\right) + \left(P_0^2/2\sigma^2\right) I_1\left(P_0^2/4\sigma^2\right) \right] \quad (4)$$

where I_1 is the modified Bessel function of first order. Note the difference between $E(P)$, the expectation value of the distribution, and $\langle P_0 \rangle$, the mean source polarization of our sample. It is clear that the expectation of P is not P_0, but a complicated expression involving P_0 and σ. This will introduce a significant bias when we try to determine P_0 by using the stacking technique.

There is also an analytic expression for the variance in both cases:

$$\mathrm{var(P)} = (4 - \pi)\sigma^2/2 \quad (5)$$

for the Rayleigh distribution and

$$\mathrm{var(P)} = 2\sigma^2 + P_0^2 - \mathrm{E}(P)^2 \quad (6)$$

for the Rice distribution, with E(P) given by equation (3). See Argüeso et al. (2009) for more details.

When we use the technique of stacking, we add up all the patches to obtain a final map. In this way, we enhance the signal-to-noise ratio. The polarization at the centre of this final stacked patch is

$$P_s = \Sigma_{k=1}^{n} P_k \quad (7)$$

with P_k the polarization at the centre of the corresponding *kth* patch. We also remove a residual background by subtracting the average of the fluxes outside the sources (those at least $3\sigma_{\mathrm{beam}}$ away from the central pixel) from the final map. Although by subtracting the off-source background we are slightly increasing the dispersion around the measured mean, as explained before, this is done to take into account the presence of residual foregrounds in our *Planck* maps in total intensity estimations and, therefore, in the patches centred at the positions of our sources (contrary to radio maps at low frequency, where these foregrounds are generally negligible). Calling P_{0k} the polarization amplitude of the source at the centre of the *kth* patch, and taking into account the subtraction of the residual background, we find the following expressions for the expectation of the polarization at the central pixel of the final stacked map and for its variance:

$$\mathrm{E}(P_s) = \Sigma_{k=1}^{n} \sigma \sqrt{\pi/2} \Big(\exp\left(-P_{0k}^2/4\sigma^2\right) \left[\left(1 + P_{0k}^2/2\sigma^2\right) I_0 \times \left(P_{0k}^2/4\sigma^2\right) + P_{0k}^2/2\sigma^2 I_1\left(P_{0k}^2/4\sigma^2\right) \right] - 1 \Big) \quad (8)$$

$$\mathrm{var}(P_s) = 2n\sigma^2 + \Sigma_{k=1}^{n}(P_{0k}^2 - \mathrm{E}(P_k)^2) + n(4 - \pi)\sigma^2/2p \quad (9)$$

where p is the number of independent beams used for the calculation of the average background. Let us suppose, for the sake of simplicity, that all the sources have the same amplitude $P_0 = m\sigma$. In that case, we can easily compute the relative error $(\mathrm{E}(P_s)/n - \langle P_0 \rangle)/\langle P_0 \rangle$ that we will make when estimating $\langle P_0 \rangle$ with P_s/n. For instance, for $m = 1, 2, 3, 4, 5$ we obtain -0.7047 , -0.4905 , -0.3602 , -0.2815 , -0.2304, respectively. As we can see, the bias is very significant.

If we carry out a *quadratic stacking* defining $P_{qs} = \Sigma_{k=1}^{n} P_k^2$ and calculate $\mathrm{E}(P_{qs}/n)$, we find

$$\mathrm{E}(P_{qs}/n) = 2\sigma^2 + \left\langle P_0^2 \right\rangle \quad (10)$$

where $\langle P_0^2 \rangle$ is the average of P_0^2 for our sample of sources. Therefore, we can determine, in theory, $\langle P_0^2 \rangle$ as

$$\left\langle P_0^2 \right\rangle = \mathrm{E}(P_{qs}/n) - 2\sigma^2 \quad (11)$$

Besides, the r.m.s deviation of P_{qs}/n can also be readily obtained

$$\mathrm{var}(P_{qs}/n) = \left(2\sigma/\sqrt{n}\right)^2 \left(\sigma^2 + \left\langle P_0^2 \right\rangle\right) \quad (12)$$

Assuming, for simplicity, that all the sources have the same amplitude $P_0 = m\sigma$ with $m = 1, 2, 3, 4, 5$, we find the following values for the r.m.s. of P_{qs}/n in terms of $\sigma^2/\sqrt{n}$: 2.8284 , 4.4721 , 6.3246 , 8.2460 , 10.1978. Thus, we can obtain a good estimation of $\langle P_0^2 \rangle$ with a low r.m.s. deviation (see Section 3).

The knowledge of $\langle P_0^2 \rangle$ allows us to estimate $\langle \Pi^2 \rangle$, an important quantity that can be found in the literature for other samples (Tucci & Toffolatti 2012) and that is used in Section 3 to characterize the lognormal distribution for Π.

This calculation cannot be directly applied to our case because the values of P_{0k} will be different for each source and, since the sources are not detected in the polarization maps, the individual information of each source about the S/N is not available. However, we can carry out simulations with injected sources and estimate the bias, as described in Section 2.4.

2.4 Source injection

In order to investigate the robustness of stacking in our analysis, we perform a source injection test. We injected simulated compact sources in our real maps, at random positions but avoiding the position of real sources. In this way, we can assess how well the method works in presence of potential systematics such as foreground contamination, noise bias and leakage.

In the sky region outside the Galactic mask, the sources in total intensity are simulated at each frequency independently following the model by Tucci et al. (2011), with a flux limit of ∼316 mJy (at 30 GHz).

As demonstrated in Stil et al. (2014), the assumed statistical distribution for the flux densities/degree of polarization has a direct effect on the measured mean polarization properties. In their work, they conclude that for their case, the best statistical distribution to be used is the one estimated directly from the detected sources of their sample. In our case, we are in a better situation because we have accurate observations of our same population of sources (for faintest sources and at slightly lower frequencies) by Massardi et al. (2013): they observed with the ATCA during a dedicated, high sensitivity run ($\sigma_P \sim 1$ mJy) a 99 per cent complete sample of extragalactic sources with $S_{20\,\mathrm{GHz}} > 500$ mJy, with declination $\delta < -30^\circ$ and a detection rate in polarization at 20 GHz of 91.4 per cent. With this sample they were able to determine that the degree of polarization of their sources follows a lognormal distribution. Therefore, considering that our compact radio sources are from the same parent

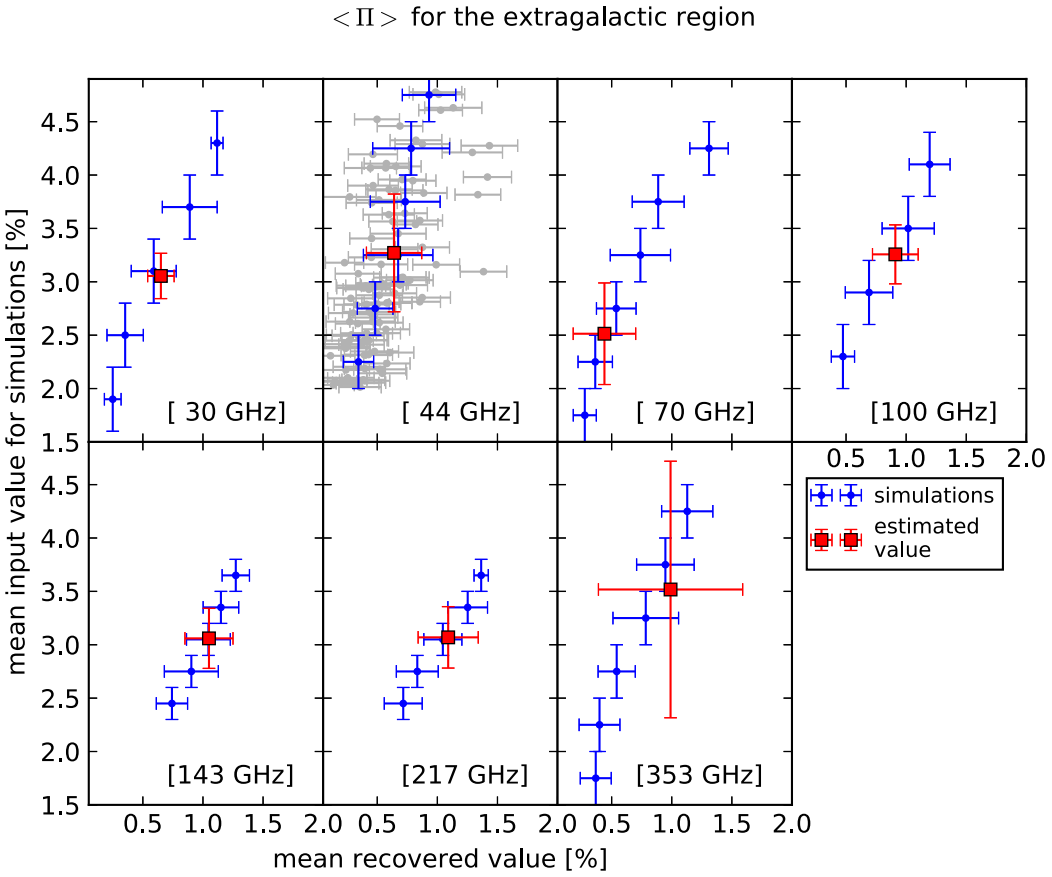

Figure 2. Results obtained outside the adopted mask (extragalactic region of the sky) from 30 to 353 GHz. As an example, in the 44 GHz panel, the grey points are obtained with each individual simulation: on the *y*-axis, we plot the mean input ⟨Π⟩ value for simulations and the *x*-axis is the value recovered with stacking for different values of μ and σ, as described in the text. For all the panels, the linear interpolation of these points gives us the correction for the noise bias that has to be applied to the observed values (red squares). The blue points are obtained by averaging over the simulations points with a binning step of about 0.5 in the *y*-axis.

population of those by Massardi et al. (2013), we can safely apply their conclusions to our sample and assume a lognormal distribution without any further analysis.

In view of the above, the flux densities in polarization are then simulated following a lognormal distribution for different values of ⟨Π⟩ in each simulation, and we assume a uniform random polarization angle to compute Q and U for each source. From the simulated catalogue, we then create the simulated sources map and convolve it with the FWHM of the instrument (which is different for each *Planck* channel) before adding it to the real Q and U maps. Finally, we construct the new P map (real P map plus injected sources) to be used in the same stacking procedure as for the real data.

As explained in Section 2.3, we need to correct our measurements from the noise bias. In order to estimate this correction, we inject simulated sources in the real maps as described above. For each simulation, we vary randomly both the *location*, μ and *scale*, σ, parameters of the lognormal distribution (see Section 2.5). At each frequency channel, we limit the range of the simulated (μ, σ) pairs by using the first tens of simulations and being guided by the measured ⟨Π⟩ values, not yet bias corrected. As a general outcome, low σ parameters produce Gaussian-like values around the μ parameter. On the contrary, high σ values create a distribution with a long tail at the high end and, as a consequence, a mean value greater than the μ parameter. In other words, if two simulations have the same location parameter, the one with the bigger scale parameter will produce more sources with high polarization degree and therefore higher recovered values.

Then, we apply the same methodology described in Section 2.2 to obtain a recovered (biased) value. We repeat this procedure for at least 100 simulations at each frequency. By comparing the theoretical simulated $\langle\Pi\rangle = \langle P_s/S_s\rangle$ with the recovered values we are able to obtain the noise bias correction relationships shown as blue points in Figs 2–5. These blue points are simply the binned values, equally spaced in the *x*-axis, of the 100 individual simulations (shown as grey points, as an example, at 44 GHz for Figs 2 and 3). Please notice that most of the dispersion is caused by the brightest sources in each simulation that can modify greatly the input and/or recovered values. Finally, we estimate our debiased measurements (red points) using a linear interpolation by means of a fit to the blue points of the derived noise bias correction relationships.

As for the simulations in the sky region inside the Galactic mask, it should be noticed that there is no source number counts model consistently describing the compact source populations inside this mask. However, we checked in the PCCS (Planck Collaboration XXVIII 2014) and in the PCCS2 that the model by Tucci et al. (2011) can still be considered a fair representation for the shape of the rough number counts for compact objects inside the adopted mask, at least for the purpose of estimating the noise bias correction with source injection. For this reason, we decide to apply the same

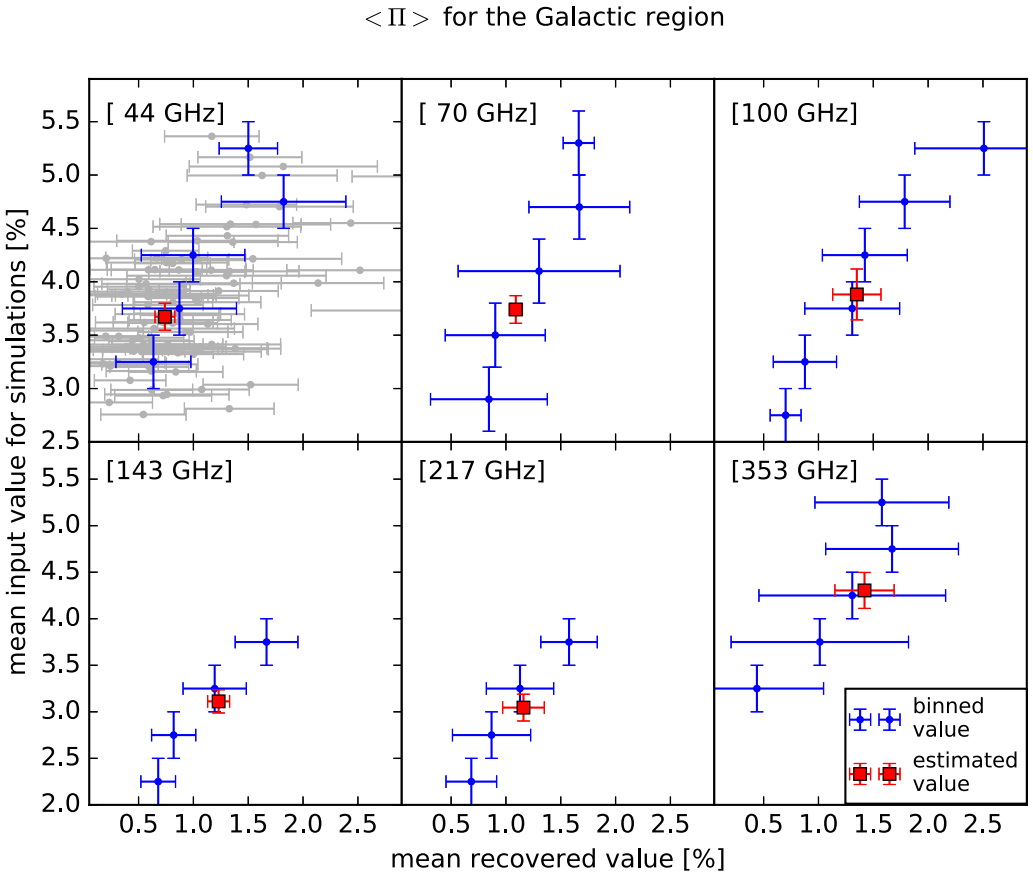

Figure 3. Results obtained inside the adopted mask (Galactic region of the sky) from 44 to 353 GHz. As in Fig. 2, the grey points in the 44 GHz panel are obtained with each individual simulation. The red squares are the values obtained with stacking on our sample's positions and corrected for the noise bias using the linear interpolation and the blue points are the binned version of the simulations points.

procedure used for compact radio sources that lay outside the mask to estimate and correct the bias.

As described in Section 2.3, $\langle\Pi^2\rangle$ should suffer of a lower contamination due to the noise bias that should be mainly taken into account by simply subtracting the mean in the stacking procedure. In any case, we compute the correction to this quantity in the same way as for $\langle\Pi\rangle$.

Moreover, *Planck* maps seem to suffer from a leakage between total intensity and polarization (Planck Collaboration II 2016). Whereas for the HFI channels this effect is negligible when estimating the polarized flux density of compact sources (see Planck Collaboration XXVI 2016), this might not be the case for the LFI ones. We use source injection to check its importance. In view of the above, we simulate the leakage of total intensity into polarization as a normal distribution with a dispersion of 0.1 for each injected source and we apply the same stacking procedure. We found that even down to the 1σ level, the leakage is not affecting our results.

Finally, to check that our findings are model independent, we also perform simulations adopting the source number count model by De Zotti et al. (2005). Comparing both sets of results we obtain that they are compatible within 1σ and, thus, we can be reasonably confident in our conclusions.

2.5 Lognormal distribution parameters

As discussed in Section 2.4, we can safely adopt a lognormal distribution when simulating the flux densities in polarization. If we assume a lognormal distribution for Π, the PDF of which is given by

$$f(\Pi;\mu,\sigma) = \frac{1}{\Pi\sigma\sqrt{2\pi}}\exp\left(-\frac{(\ln(\Pi)-\mu)^2}{2\sigma^2}\right) \quad (13)$$

we use $\langle\Pi\rangle$ and $\langle\Pi^2\rangle$ for the determination of μ and σ. Following Crow & Shimizu (1988), they are given by

$$\mu = \ln\left(\frac{\langle\Pi\rangle^2}{\sqrt{\langle\Pi^2\rangle}}\right) \quad (14)$$

$$\sigma = \sqrt{\ln\left(\frac{\langle\Pi^2\rangle}{\langle\Pi\rangle^2}\right)} \quad (15)$$

and their errors are, respectively

$$\mathrm{var}(\mu) = \frac{4}{\langle\Pi\rangle^2}\mathrm{var}(\langle\Pi\rangle) + \frac{1}{\langle\Pi^2\rangle}\mathrm{var}\left(\sqrt{\langle\Pi^2\rangle}\right) \quad (16)$$

$$\mathrm{var}(\sigma) = \frac{1}{\sigma^2}\left(\frac{\mathrm{var}(\langle\Pi\rangle)}{\langle\Pi\rangle^2} + \frac{1}{\langle\Pi^2\rangle}\mathrm{var}\left(\sqrt{\langle\Pi^2\rangle}\right)\right) \quad (17)$$

From μ, we can then compute the median fractional polarization as

$$\Pi_m = \exp(\mu) \quad (18)$$

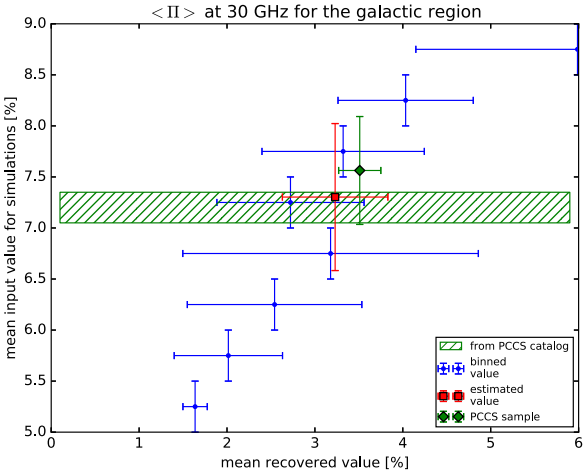

Figure 4. Galactic region results at 30 GHz. The blue points are from the binned version of the simulations results: input ⟨Π⟩ values on the *y*-axis and recovered ⟨Π⟩ values with stacking on the *x*-axis. The red square is the value obtained with stacking on our Galactic sample positions (*x*-axis) and the corrected value (*y*-axis), according to the linear interpolation. The green diamond is the result obtained with the subsample $P > 2P_{\rm err}$ in the PCCS2 catalogue to be compared with the green hatched stripe (actual value computed with the PCCS2 flux densities for the same subsample).

Therefore, from the recovered values of ⟨Π⟩ and ⟨Π^2⟩ we can compute the parameters μ and σ characterizing the adopted distribution.

3 RESULTS

Of the 1560 sources in our sample, 881 are outside the *Planck* GAL60 (plus the MCs regions) mask and 679 are inside it. In both cases, we have a fairly good sample. In these positions, we perform stacking in the *Planck* channels from 30 to 353 GHz both in total intensity and polarization. From the patches resulting from the stacking, we estimate ⟨S⟩, ⟨P_0⟩, ⟨Π⟩ and ⟨S^2⟩, ⟨P_0^2⟩, ⟨Π^2⟩ and we compute the errors from the standard deviation of the residual background fluctuations, as described in Section 2.2. The results are summarized in the left part of Tables 1 and 2.

To estimate ⟨Π⟩ from the bias-uncorrected values, we use the procedure described in Section 2.4, whose results are shown in Fig. 2 for the extragalactic region and in Fig. 3 for the Galactic region of the sky. The grey points in the 44 GHz panel are the 100 simulations (the inputs are on the *y*-axis and the recovered values with stacking are on the *x*-axis). For all the panels, the blue points are obtained by binning the simulations results with a binning step of about 0.5 in the *y*-axis. The red squares are the values recovered with data, namely performing stacking in the PCCS2 30 GHz positions: these results are computed by performing a linear interpolation to

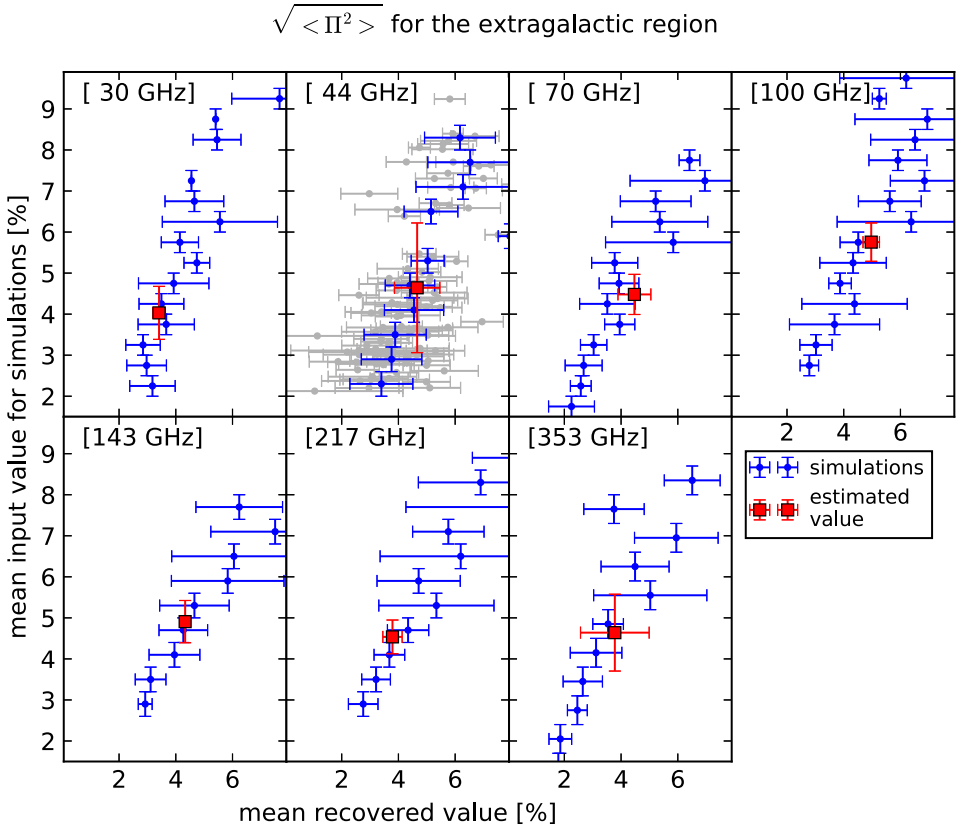

Figure 5. Results obtained for $\sqrt{\langle\Pi^2\rangle}$ outside the adopted mask (extragalactic region of the sky) from 30 to 353 GHz. As an example, in the 44 GHz panel, the grey points are obtained with each individual simulation: the *y*-axis is the mean input $\sqrt{\langle\Pi^2\rangle}$ for simulations and the *x*-axis is the value recovered with stacking for different values of μ and σ, as described in the text. For all the panels, the linear interpolation of these points gives us the correction for the noise bias that has to be applied to the observed values (red squares). The blue points are obtained by averaging over the simulations points with a binning step of about 0.5 in the *y*-axis.

Table 1. From left to right: frequency, mean fractional polarization with r.m.s. errors uncorrected and corrected for the noise bias, square root of the mean quadratic fractional polarization with 1σ errors uncorrected and corrected for the noise bias, μ and σ parameters of the lognormal function characterizing the mean fractional polarization distributions (see text) and their 1σ errors. The results are for the case outside the *Planck* Galactic mask with $f_{\rm sky} = 60$ per cent and the background fit as described in the text.

	Extragalactic region											
	Uncorrected		Corrected		Uncorrected		Corrected		Lognormal parameters			
Freq [GHz]	$\langle\Pi\rangle$ per cent	Error per cent	$\langle\Pi\rangle$ per cent	Error per cent	$\sqrt{\langle\Pi^2\rangle}$ per cent	Error per cent	$\sqrt{\langle\Pi^2\rangle}$ per cent	Error per cent	μ	Error	σ	Error
30	0.65	0.11	3.05	0.21	3.41	0.22	4.03	0.65	0.8	0.2	0.7	0.2
44	0.64	0.23	3.27	0.55	4.66	0.80	4.64	1.58	0.8	0.5	0.8	0.4
70	0.44	0.26	2.51	0.48	4.47	0.58	4.48	0.49	0.3	0.4	1.1	0.2
100	0.91	0.19	3.26	0.28	4.97	0.29	5.75	0.47	0.6	0.2	1.1	0.1
143	1.05	0.20	3.06	0.28	4.33	0.18	4.91	0.51	0.6	0.2	1.0	0.1
217	1.09	0.25	3.07	0.29	3.79	0.34	4.54	0.41	0.7	0.2	0.9	0.1
353	0.99	0.60	3.52	1.20	3.78	1.21	4.64	0.94	1.0	0.7	0.7	0.5

Table 2. From left to right: frequency, mean fractional polarization with 1σ errors uncorrected and corrected for the noise bias. The results are for the case inside the *Planck* Galactic mask with $f_{\rm sky} = 60$ per cent and the background fit as described in the text.

	Galactic region			
	Uncorrected		Corrected	
Freq [GHz]	$\langle\Pi\rangle$ per cent	Error per cent	$\langle\Pi\rangle$ per cent	Error per cent
30	3.23	0.60	7.30	0.72
44	0.74	0.09	3.67	0.13
70	1.09	0.06	3.74	0.13
100	1.35	0.22	3.88	0.24
143	1.23	0.10	3.11	0.12
217	1.16	0.19	3.05	0.14
353	1.42	0.27	4.30	0.19

the values obtained with simulations and using it to correct/debias the measured $\langle\Pi\rangle$ (see Section 2.3).

Due to the stronger foreground contamination inside the Galactic region at 30 GHz (synchrotron emission), our individual measurements of the simulated data suffer from a much larger dispersion. The results at this frequency are shown in Fig. 4. As described in more detail in Section 3.1, at 30 GHz we are able to perform a direct check of our results, i.e. our correction procedure, that confirms that even with such high level of measurement dispersion we are still able to get acceptable results.

In the extragalactic region of the sky, the noise bias correction for $\langle\Pi\rangle$ goes approximately from 3 to 6, which corresponds to compact sources with a polarization value that presents an S/N of about 0.5–1.5, as discussed in Section 2.3. These S/N levels are the expected ones, since most of the sources are not directly detected in polarization with *Planck*. The same approach as described in Section 2.4 has been applied to correct also the values obtained for $\langle\Pi^2\rangle$ (in the extragalactic region of the sky; see Fig. 5).

As anticipated in Section 2.3 the noise bias correction for $\sqrt{\langle\Pi^2\rangle}$ is much lower than for the $\langle\Pi\rangle$ case: we find a mean value of 1.2 to be compared with 4.1 for $\langle\Pi\rangle$, in the extragalactic region of the sky.

Figs 6 and 7 are a summary of the noise bias corrected results on $\langle\Pi\rangle$ and $\sqrt{\langle\Pi^2\rangle}$ we obtain with stacking.

Fig. 6 shows the estimated $\langle\Pi\rangle$ for the different cases. In the top panel (sky region outside the Galactic mask), we compare the results obtained by subtracting the estimation of the mean value of the background from the source flux density in total intensity (green squares) with those obtained by subtracting the model of the background, as described in Section 2.2 (blue circles). In both cases the results are compatible within 1σ level. From the results in the extragalactic region, it can be concluded that all the estimated values of $\langle\Pi\rangle$ are almost consistent within one sigma for all the channels (with a weighted mean value of 3.08 per cent).

The central panel shows the same comparison, but for the sky region inside the adopted mask. Again, the results obtained by modelling the background (blue circles) or directly estimating its mean value (green squares) are consistent with each other within the errors. $\langle\Pi\rangle$ seems to remain constant across the range of frequencies from 44 to 353 GHz (with a weighted mean equal to 3.51 per cent), while at 30 GHz it reaches much higher values (7.30 $\pm$ 0.72) per cent.

Finally, in the bottom panel, we compare our results inside (red squares) and outside (black circles) the Galactic mask. With the exception of the 30 GHz channel, there is no relevant statistical difference between the values obtained inside and outside the adopted mask.

In the top panel of Fig. 7, we show the results for $\sqrt{\langle\Pi^2\rangle}$ at each frequency for the extragalactic region of the sky. In both figures, we show the 1σ error resulting from the interpolation procedure.

As described in Section 2.5, from the recovered values of $\langle\Pi\rangle$ and $\langle\Pi^2\rangle$ we compute the parameters μ and σ for the lognormal distribution in the extragalactic region and they are summarized in Table 1.

In the bottom panel of Fig. 7, we compare the median and the mean values for the estimated polarization fraction. As expected for a lognormal distribution, the values for the median are lower than those for the mean in the region outside the Galactic mask.

The foreground fluctuations inside the adopted Galactic mask affect more severely the $\sqrt{\langle\Pi^2\rangle}$ measurements producing huge dispersion between the different simulations. For this reason we decided not to attempt any $\sqrt{\langle\Pi^2\rangle}$ measurements or noise bias correction and, as a consequence, any estimation of the μ and σ parameters of the adopted lognormal distribution.

3.1 Comparison with results based on detected extragalactic compact sources

At lower frequencies, Massardi et al. (2008) – by exploiting the *Bright Source Sample* that consists of sources with $S_{20\,\rm GHz} > 500$ mJy selected in the AT20G survey (Murphy et al. 2010) and observed with the ATCA – found a $\langle\Pi\rangle$ value of 2.5 per cent at ∼20 GHz and a slight increase of Π with

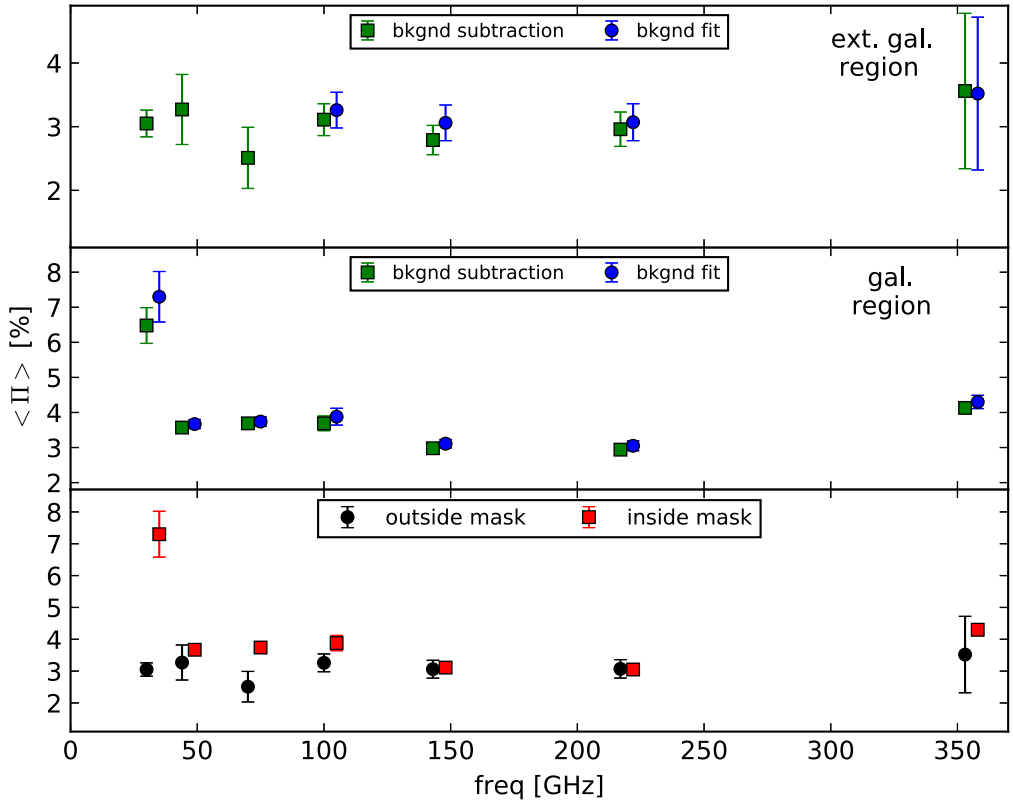

Figure 6. Mean fractional polarization for each frequency outside (top) and inside (centre) the *Planck* Galactic mask with $f_{\rm sky} = 60$ per cent. The green squares are obtained with the flat background estimation, the blue circles with the background fit as described in the text. The bottom panel compares the results obtained outside (black circles) and inside (red squares) the mask.

frequency (between 4.8 and 20 GHz) and little correlation between polarized and total intensity spectra. Moreover, Massardi et al. (2013) with sources selected again from the AT20G survey and with $S_{20\,\rm GHz} > 500$ mJy found in the same range of frequencies no significant evidence of correlation between Π and frequency or Π and total flux density and they recovered a value for ⟨Π⟩ of 2.79 per cent at 18 GHz. This value is close to the one we found in the extragalactic region at 30 GHz (3.05 ± 0.21) per cent. Sajina et al. (2011) observed with the Very Large Array, for frequencies from 4.86 to 43.34 GHz, typical values for ⟨Π⟩ of 2–5 per cent in a sample of sources selected in the AT20G catalogue with $S_{20\,\rm GHz} > 40$ mJy. More recently, Galluzzi et al. (2017) found a median value for the polarization fraction of 2.01 per cent at 33 GHz for their sample of 53 sources selected from the *faint PACO sample* (Bonavera et al. 2011), with $S_{20\,\rm GHz} > 200$ mJy. They also found no trend with frequency or flux densities (up to 38 GHz) for Π, in agreement with our current findings.

At 30 GHz, we perform a test with the PCCS2 catalogue to check that our noise bias correction is properly taken into account as described in Section 2.3. We compute ⟨Π⟩ for a subsample of our sources that are detected in polarization and have $P > 2P_{\rm err}$ where P is the polarized flux density and $P_{\rm err}$ is the error measurement in the PCCS2 (this subsample consists of 53 sources). We recover a value for the mean fractional polarization ⟨Π⟩ of (7.56 ± 0.53) per cent (green diamond in Fig. 4), in agreement with the value computed with the PCCS2 official catalogue for the same subample: (7.20 ± 0.15) per cent (green band). It is worth mentioning that this subsample is mostly made up of sources inside the Galactic mask and its ⟨Π⟩ value is very close to the one found for our sample inside the adopted mask (7.30 ± 0.72) per cent implying that probably the brightest sources in polarization in the Galactic plane are also the ones with the higher mean fractional polarization.

For frequencies higher than 40 GHz, Tucci & Toffolatti (2012) gave a preliminary estimate of $\sqrt{\langle\Pi^2\rangle}$: 3.5–4.6 per cent for FRSQ and 4.2-5.5 per cent for BL Lac, in general agreement with our findings. This agreement is not surprising, since this quantity depends on the tail of the distribution for Π, where most of the sources included in the catalogues used by these authors usually lie. On the other hand, the values of Π_m estimated by Tucci & Toffolatti (2012) are a bit higher than ours (2.5–3.6 per cent for FSRQ and 3.0-4.3 per cent for BL Lac), probably due to the fact that our measurements are based on fainter sources (in polarization) with respect to the ones in the catalogues used by them.

Moreover, López-Caniego et al. (2009) found lower ⟨Π⟩ values for *WMAP* 5-yr data (1.7, 0.91, 0.68, 1.3 per cent from 23 to 61 GHz, respectively). For the PCCS2, we compute the following values for ⟨Π⟩: 5.6, 7.9, 7.8, 6.5, 8.2 and 12.2 per cent at 30, 44, 70, 100, 143 and 217 respectively, in agreement with fig. 5 in Planck Collaboration XXVI (2016). These higher values of ⟨Π⟩, directly calculated from the PCCS2,[2] can be explained by taking into account that these same values are not estimated from a complete sample but

[2] In this case, we have used *all* the sources present in the PCCS2 for which a flux in total polarization, P, was measured. On the contrary, the estimate displayed by a green diamond in Fig. 4 is calculated only from PCCS2 sources for which $P > 2P_{\rm err}$).

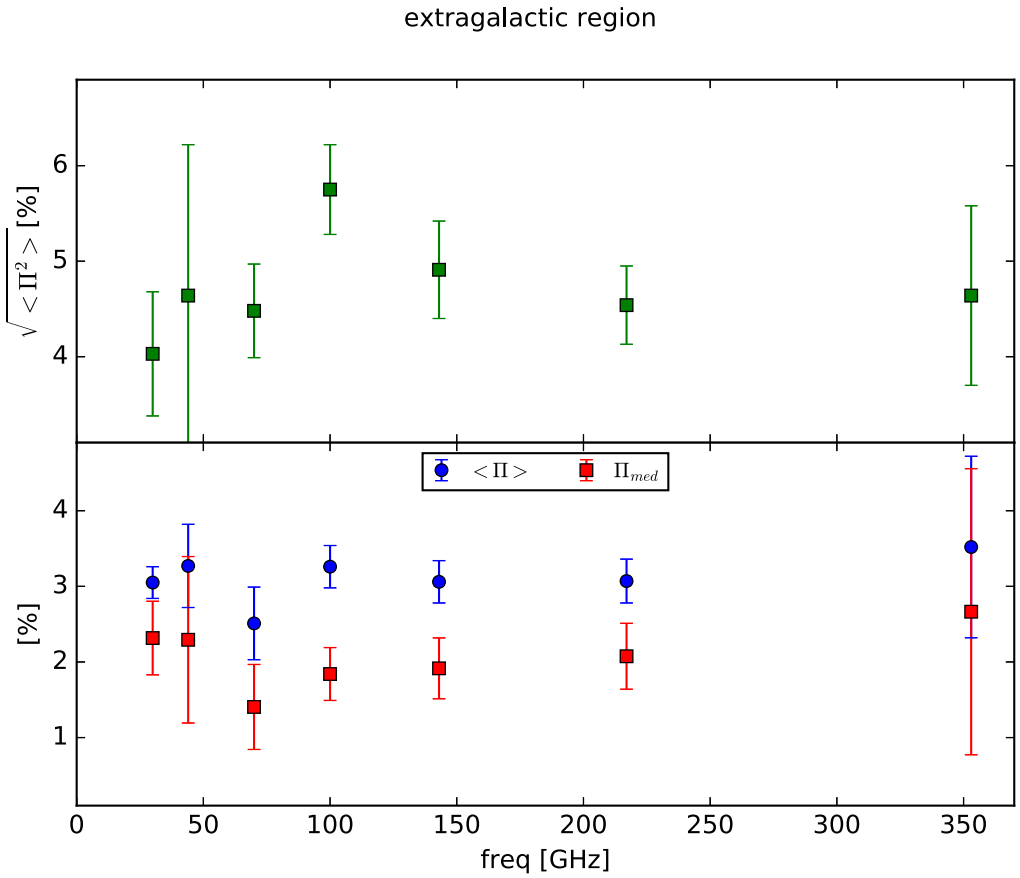

Figure 7. Top panel: $\sqrt{\langle\Pi^2\rangle}$ for the extragalactic region of the sky (green squares). Bottom panel: comparison between the mean fractional polarization (blue circles) and the median fractional polarization (red squares).

from sources that can be detected at only one particular frequency and are, thus, biased towards sources with higher polarization.

On the contrary, the stacking analysis allows us to reduce the background noise and enhance the signal. In this way we are able to compute $\langle\Pi\rangle$ at different frequencies for the *same* sample of sources, identified by their positions, regardless of whether they can be detected or not. Moreover, we also make a distinction between Galactic and extragalactic regions of the sky.

Concerning the values we found for the lognormal distribution of Π, we can compare our 30 GHz results with those by Massardi et al. (2013) at 18 GHz. They found a value for σ of 0.90 and a median polarization fraction Π_m of 2.14 per cent. They are in good agreement with our findings: $\sigma = (0.7 \pm 0.2)$ and $\Pi_m = (2.2 \pm 0.4)$ per cent (given by $\Pi_m = \exp(\mu)$).

4 CONCLUSIONS

In this work, we apply stacking to estimate the mean fractional polarization of radio sources at *Planck* frequencies. Our sample consist of 1560 sources, i.e. the sources in the PCCS2 catalogue at 30 GHz. They are divided into two subsamples: 679 inside and 881 outside the *Planck* Galactic mask with $f_{\rm sky} = 60$ per cent. At higher *Planck* frequencies, the positions in the sky corresponding to these sources are used. $\langle\Pi\rangle$ is computed at 30, 44, 70, 100, 143, 217 and 353 GHz in the *Planck* maps.

Due to detection bias, we perform background subtraction to compute the mean flux density in total intensity for the sources in two different ways (see Section 2.2): by subtracting the mean value obtained in the region of the patch $3\sigma_{\rm beam}$ away from its the centre and by modelling the background before its subtraction. In both cases, we find compatible results (within their errors).

When we use the stacking technique to enhance the signal, we find that there is a significant bias in the determination of the average source polarization (called noise bias, see Section 2.3). In order to estimate and correct for this bias, we perform simulations with injected sources (Section 2.4).

We also perform simulations by following two different source counts models (De Zotti et al. 2005; Tucci et al. 2011). The results are compatible at the 1σ level.

For the sky region outside the Galactic mask, we obtain values for $\langle\Pi\rangle$ in the different channels that are not too different taking into account their errors: they go from the lowest value of (2.51 ± 0.48) per cent at 70 GHz up to (3.52 ± 1.20) per cent at 217 GHz. Remarkably, there is a good agreement with low-frequency survey results: 2.5 per cent by Massardi et al. (2008), 2.79 per cent by Massardi et al. (2013) and 2-5 per cent by Sajina et al. (2011).

We also estimate the parameters characterizing the lognormal distribution for Π: we obtain a weighted mean for μ over the whole *Planck* frequency range of 0.7 (that would imply a median value for Π of 1.9 per cent, lower than the measured mean value of 3.08 per cent, as expected for a lognormal distribution) and a weighted mean for σ of 1.0.

For the region inside the Galactic mask, the behaviour is similar to the previous case with a tendency to slightly higher values. $\langle\Pi\rangle$ ranges from a minimum value of (3.05 ± 0.14) per cent at 217 GHz to a maximum of (4.30 ± 0.19) per cent at 353 GHz, with the

exception of the 30 GHz channel, where ⟨Π⟩ is much higher, reaching a value of (7.30 ± 0.72) per cent.

This excess of polarization is not seen in our source injection test and therefore indicates a stronger emission in polarization that, apparently, only affects frequencies lower than 30 GHz in the Galactic region. The fact that the measured mean of the full sub-sample inside the Galactic region is very similar to the value measured considering only the sources detected at 30 GHz in polarization, implies that these few very bright sources completely dominate the signal. Therefore, the value measured directly from the PCCS2 cannot be considered a correct statistical representation of the subsample properties.

The strong contamination produced by the diffuse emission of our Galaxy inside the Galactic region does not allow us to estimate $\sqrt{\langle\Pi^2\rangle}$ and its bias corrections and, therefore, the lognormal distribution parameters. Considering these limitations and taking into account the approximations adopted to simulate the source population in this sky region, it is clear that the Galactic region results are less robust than the extragalactic region ones, but of great interest in any case.

In conclusion, the stacking method can be useful to estimate the mean and median values of the fractional polarization of mainly undetected compact sources by exploiting the knowledge of their positions in the sky. At the lowest *Planck* frequencies and at high Galactic latitudes, our present results are in general agreement with other published works on ERS (Sajina et al. 2011; Massardi et al. 2013; Galluzzi et al. 2017). At higher frequencies, we are presenting novel results that could be useful in estimating the polarized source number counts and, consequently, the contamination due to these sources for the detection of the primordial CMB E and B mode polarization. Therefore, our results are very useful when planning future CMB experiments in polarization such as *CORE* (André et al. 2014).

ACKNOWLEDGEMENTS

We thank the anonymous referee for the insightful comments and remarks that helped a lot in improving the original paper and for the careful reading of the manuscript. We also thank M. López-Caniego and B. Partridge for useful comments.

We acknowledge financial support from the I+D 2015 project AYA2015-65887-P (MINECO/FEDER). JGN also acknowledges financial support from the Spanish MINECO for a 'Ramon y Cajal' fellowship (RYC-2013-13256).

REFERENCES

André P., Baccigalupi C., Banday A., 2014, J. Cosmol. Astropart. Phys., 2, 006
Argüeso F., Sanz J. L., Herranz D., López-Caniego M., González-Nuevo J., 2009, MNRAS, 395, 649
Banfield J. K., George S. J., Taylor A. R., Stil J. M., Kothes R., Scott D., 2011, ApJ, 733, 69
Bennett C. L. et al., 2003, ApJ, 583, 1
Béthermin M. et al., 2012, A&A, 542, A58
BICEP2/Keck and Planck Collaborations, 2015, Phys. Rev. Lett. 114, 101301
BICEP2 Collaboration, 2016, ApJ, 833, 228
Bonavera L., Massardi M., Bonaldi A., González-Nuevo J., de Zotti G., Ekers R. D., 2011, MNRAS, 416, 559
Condon J. J., Cotton W. D., Greisen E. W., Yin Q. F., Perley R. A., Taylor G. B., Broderick J. J., 1998, AJ, 115, 1693
Crow E. L., Shimizu K., 1988, Lognormal Distributions. Theory and Applications. Marcel Dekker Inc., New York
De Zotti G., Ricci R., Mesa D., Silva L., Mazzotta P., Toffolatti L., González-Nuevo J., 2005, A&A, 431, 893
De Zotti G. et al., 2015, J. Cosmol. Astropart. Phys., 6, 018
De Zotti G. et al., 2016, JCAP, preprint (arXiv:1609.07263)
Dole H. et al., 2006, A&A, 451, 417
Galluzzi V. et al., 2017, MNRAS, 465, 4085
Jackson N., Browne I. W. A., Battye R. A., Gabuzda D., Taylor A. C., 2010, MNRAS, 401, 1388
López-Caniego M. et al., 2009, ApJ, 705, 868
Marsden G. et al., 2009, ApJ, 707, 1729
Massardi M. et al., 2008, MNRAS, 384, 775
Massardi M. et al., 2011, MNRAS, 412, 318
Massardi M. et al., 2013, MNRAS, 436, 2915
Mesa D., Baccigalupi C., De Zotti G., Gregorini L., Mack K.-H., Vigotti M., Klein U., 2002, A&A, 396, 463
Murphy T. et al., 2010, MNRAS, 402, 2403
Papoulis A., 1984, Probability, Random Variables and Stochastic Processes. McGraw Hill, New York
Planck Collaboration I, 2016, A&A, 594, A1
Planck Collaboration II, 2016, A&A, 594, A2
Planck Collaboration XI, 2016, A&A, 594, A11
Planck Collaboration XIII, 2011, A&A, 536, A13
Planck Collaboration XIII, 2016, A&A, 594, A13
Planck Collaboration XIX, 2014, A&A, 571, A19
Planck Collaboration XXVI, 2016, A&A, 594, A26
Planck Collaboration XXVIII, 2014, A&A, 571, A28
Rice H. C., 1954, in Wax N. ed., Selected Papers on Noise and Stochastic processes. Dover Publication, New York, p. 133
Sadler E. M. et al., 2006, MNRAS, 371, 898
Sajina A. et al., 2011, ApJ, 732, 45
Simmons J. F. L., Stewart B. G., 1985, A&A, 142, 100
Stil J. M., Keller B. W., George S. J., Taylor A. R., 2014, ApJ, 787, 99
Tucci M., Toffolatti L., 2012, Adv. Astron., 2012, 624987
Tucci M., Martínez-González E., Toffolatti L., González-Nuevo J., De Zotti G., 2004, MNRAS, 349, 1267
Tucci M., Toffolatti L., de Zotti G., Martínez-González E., 2011, A&A, 533, A57
Vidal M., Leahy J. P., Dickinson C., 2016, MNRAS, 461, 698

This paper has been typeset from a TEX/LATEX file prepared by the author.